Thermal Degradation Studies on Rigid Polyurethane Foams Blown with Pentane

Krzysztof Pielichowski,[1] Kamil Kulesza,[1] Eli M. Pearce[2]

[1] *Department of Chemistry and Technology of Polymers, Technical University, ul. Warszawska 24, 31-155 Kraków, Poland*
[2] *Polymer Research Institute, Polytechnic University, Six MetroTech Center, Brooklyn, New York 11201*

Received 29 August 2001; accepted 9 September 2002

ABSTRACT: The effect of sodium dihydrogenphosphate, trisodium pyrophosphate, and sodium aluminocarbonate on the thermal decomposition of rigid polyurethane (PUR) foams, based on diphenylmethane-4,4-diisocyanate, diphenyl-2,2-propane-4,4-dioxyoligo(ethylene oxide), and oxyalkylenated toluene-2,6-diamine, blown with pentane, was studied. Thermogravimetric (TG) data have shown that there is a stabilization effect of additives in the initial stage of degradation, both in nitrogen and air atmosphere, and the decomposition proceeded in two steps up to 600°C. Results of the kinetic analysis by the isoconversional methods of Ozawa–Flynn–Wall and Friedman yielded values of (apparent) activation energy (E_a) and preexponential factor (A). For phosphate-stabilized PUR samples, E_a remained stable over a broad area of the degree of conversion, while for carbonate-containing sample two regions of E_a were observed. Further advanced kinetic analysis by a nonlinear regression method revealed the form of kinetic function that was the best approximation for experimental data—for a two-stage consecutive reaction the first step was the Avrami–Erofeev nucleation-dependent model, and the second step was a chemical reaction (1st or nth order) model. The integrated thermogravimetric (TG)/Fourier transform infrared (FTIR) technique probed the thermal degradation of modified PURs by analyzing the evolved gases. The solid residue remaining at different temperatures was identified by diffuse reflection FTIR (Kubelka–Munk format). The complex thermal behavior was discussed on the basis of the obtained results—it can be shown that the global stabilization effect is a multistage process whose initial conditions are of critical importance in governing the nature of the entire process.
 J Appl Polym Sci 88: 2319–2330, 2003

Key words: rigid polyurethane foams; stabilization; thermal properties

INTRODUCTION

Polyurethanes (PURs) are a class of polymers with an extremely versatile range of properties and applications. Some of the most important polyurethane-based materials are rigid polyurethane (PUR) foams that are commonly used for building engineering applications and for thermal insulation in domestic and commercial refrigeration, as well as furniture components and decorative paneling.[1,2] However, these polymeric materials have relatively low thermal stability, primarily due to the presence of urethane bonds. The energy of dissociation of the urethane groups is influenced by the substituents (structural units) bound to oxygen and nitrogen atoms in the urethane group. Bayer reported that the upper stability temperatures for the different urethane groups depends on their activation energy and lay between 120 and 250°C.[3] Besides, thermal studies on polyurethane materials are complicated by one or more of the following effects: (1) specific intermolecular interactions via hydrogen bonding, (2) crystallinity, and (3) the presence of chemical crosslinking. All three effects may influence the nature and extent of thermal decomposition, and the possibility of inhibiting it by using thermal stabilizers. Their mode of action is still a subject of debate—for example, in spite of many studies performed on haloalkyl phosphates, little is certain about their site of action (condensed or vapor phase) and the mechanism of their effect on PUR stability.[4] Hence, one proposed mechanism often cited is based on activity in the condensed phase and involves the thermal degradation of the phosphorus compound to phosphoric or polyphosphoric acids. These acids and the char, the formation of which they are said to catalyze, are stated to form barriers that attenuate the transfer of heat from the decomposition zone to the substrate as well as the transport of fuel in the reverse direction.[5] Grassie and Zulfiqar stated that phosphoric acid reacts very efficiently with the carbodiimide formed by the condensation of the isocyanate released on the thermolysis of the polyurethane, and that this leads to crosslinking and could present a mechanism of char formation.[6] On

Correspondence to: K. Pielichowski (kpielich@usk.pk.edu.pl).
Contract grant sponsor: Kosciuszko Foundation, New York (K.P.).

the other hand, in a study performed by Benbow and Cullis, most of the haloorganophosphates were found to volatilize quantitatively before the polymer begins to degrade, which implies activity in the vapor phase.[7] Since the picture obtained from the literature is contradictory and confusing, we decided to perform a systematic study (including advanced multistage kinetic analysis) on the thermal stability of rigid polyurethane foams, modified by well-defined novel stabilizers.

EXPERIMENTAL

Materials

1. Partially polymerized diphenylmethane-4,4-diisocyanate (PMDI), produced by ICI Ltd., Everberg, Belgium.

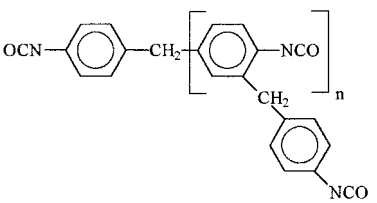

2. Diphenyl-2,2-propane-4,4-dioxyoligo(ethylene oxide) (ICSO, Kedzierzyn-Kozle, Poland).

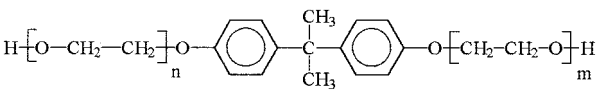

n + m = 3 to 7

3. Oxyalkylenated toluene-2,6-diamine (Alfa Systems, Brzeg Dolny, Poland).

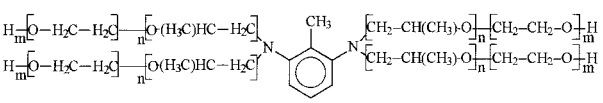

n, m = 0 or 1

4. *N,N*-Dimethylcyclohexylamine (DMCHA) (Texaco Chemical Deutschland GmbH, Düsseldorf, Germany).
5. Pentane (75% *n*-pentane in mixture with isopentane), Petrolchemisches Kombinat, Schwedt, Germany.
6. Silicon oil (SR-321, Union Carbide, Marietta, GA).
7. Trisodium pyrophosphate, $Na_3HP_2O_7$ (Chemical Works, Alwernia, Poland).
8. Sodium dihydrogenphosphate, NaH_2PO_4 (Chemical Works, Alwernia, Poland).
9. Sodium aluminocarbonate, $Na_2Al_2(CO_3)_2O_2$ (Technical University, Krakow, Poland).

PUR foam formulation

First, a polyol premixture was prepared by mixing together diphenyl-2,2-propane-4,4-dioxyoligo(ethylene oxide) (58.42 wt %), oxyalkylenated toluene-2,6-diamine (30.00 wt %), silicon oil (1.84 wt %), and water (0.74 wt %). The amounts of components were chosen as optimal after a series of test experiments. Then, appropriate amounts of DMCHA catalyst, pentane (a mixture of 75 wt % *n*-pentane with 2-methylbutane) blowing agent, and additive (trisodium pyrophosphate, sodium dihydrogenphosphate, or sodium aluminocarbonate) were added to the premixture and stirred for 60 s. At the next stage, the isocyanate component was added; the components were stirred for 10 s with an overhead stirrer and then the mixture was dropped into an open mould (in the shape of rectangular prism 150 × 150 × 100 mm) lined with paper. The formulation used for the rigid polyurethane foam preparation is presented in Table I.

TABLE I
Formulation of the Rigid Polyurethane Foam

Component	Mass ratio of given component to the total mass of foam (wt %)		
Fire retardant	0	10	20
Polyol premixture	56,16	50,54	44,92
DMCHA	0,19	0,17	0,15
Pentane	4,79	4,31	3,83
PMDI	38,86	34,98	31,09

Samples under investigation were as follows:

Sample 1: base foam (no additive).
Sample 2: foam with 20% of sodium dihydrogenphosphate.
Sample 3: foam with 20% of trisodium pyrophosphate.
Sample 4: foam with 10% of sodium aluminocarbonate.

Techniques

Thermogravimetric analysis

Thermogravimetric analysis (TGA) was performed on a TA Instruments TGA 2950 thermal analyzer, operating in a dynamic mode at a heating rate of 2.5, 5, 10, and 20 K/min. The conditions were as follows: sample weight, ~2 mg; atmosphere, nitrogen or air, open α-Al_2O_3 pan. The raw data were converted to ASCII files and kinetic analysis was carried out using an in-house program and a Netzsch Thermokinetic Program (v. 99/10) on an IBM-compatible computer with Pentium III processor.

TGA coupled with fourier transform infrared spectroscopy

Thermogravimetric analysis coupled with Fourier transform infrared spectroscopy (FTIR) was carried out using a Mettler-Toledo TGA/SDTA™ (Single Differential Thermal Analysis) 851 thermal analyzer (heating rate = 20 K/min, sample weight ~ 2 mg,

nitrogen flow = 50 cm^3/min) and a Jasco 610 FTIR spectrometer. The thermogravimetric analyzer and spectrometer were suitably coupled to enable the passage of evolved products from the furnace to the gas cell over a short path, to minimize secondary reaction or condensation on cell walls. Moreover, the experimental conditions have been chosen to ensure that the condensable products form a submicron aerosol mist. This size aerosol has two advantages: (1) the particles follow the gas stream lines, thus minimizing condensation; and (b) the particles produce little scattering in the mid-IR, so the condensable products can be analysed online in the FTIR cell.

Diffuse reflectance infrared fourier transform spectroscopy

Diffuse reflectance infrared Fourier transform spectroscopy (DRIFTS) spectra were taken on a Perkin–Elmer 1600 FTIR spectrometer, equipped with a DR unit. Samples were used as received after TG analysis; DRIFTS data were presented in the Kubelka–Munk format.

RESULTS AND DISCUSSION

Thermal analysis

Thermogravimetric (TG) results of samples under investigation in nitrogen are shown in Figure 1.

Degradation process starts at ca. 160–200°C and proceeds in one (sample 1) or two (samples 2–4) steps; at 500°C decomposition can be considered as being completed. Detailed TG data of the initial stage of decomposition are summarized in Table II.

TABLE II
Temperatures (°C) at Which Weight Loss Reached the Levels Specified on Heating in Nitrogen at 10°/min Measured by TG

Sample	$T_{1\%}$ (°C)	$T_{3\%}$ (°C)	$T_{5\%}$ (°C)	$T_{10\%}$ (°C)	$T_{20\%}$ (°C)
1	83	157	186	236	277
2	143	202	235	266	292
3	118	183	206	258	290
4	112	180	200	231	254

In the atmosphere of air, we can observe another course of the degradation process—Figure 2.

For all the samples there is a distinct second decomposition step that commences at ca. 350°C. The onset of decomposition (Table III) shows the influence of phosphate-based additives.

Analysis of the 1st derivative of the TG curve (DTG) indicates that first maximum occurs at 280–300°C for all the samples; then second maximum at ca. 520°C (except for sample 4) is present.

Based on the TG traces, it can be seen that additives influence the thermal stability of PURs (at the beginning of decomposition) in the following order: sample 2 > sample 3 > sample 4 > sample 1.

Kinetic analysis

Kinetic parameters from TGA data may yield additional insight into the mechanism of decomposition of polyurethanes. Hence, Chang et al. calculated the activation energy (E_a) of the degradation process of a series of copolyurethanes with various phosphorus contents by using Ozawa and Flynn methods.[8] It has been shown that E_a changes with the degree of con-

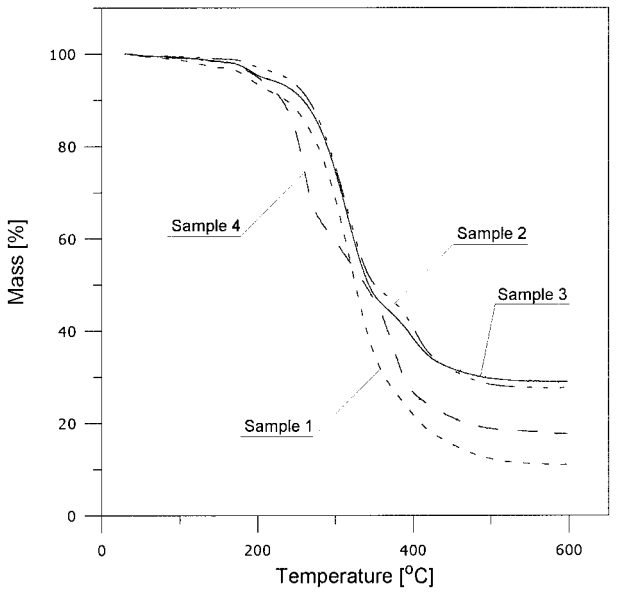

Figure 1 TG curves of samples 1–4 at 10°/min under nitrogen.

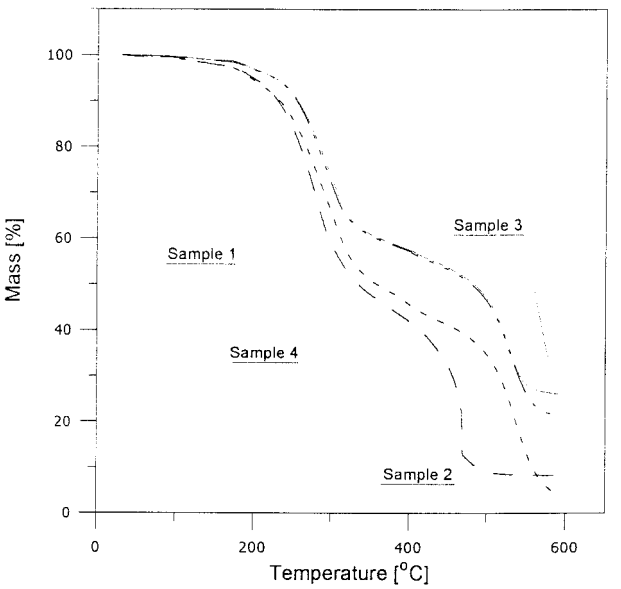

Figure 2 TG curves of samples 1–4 at 10°/min under air.

TABLE III
Temperatures (°C) at Which Weight Loss Reached the Levels Specified on Heating in Air at 10°/min Measured by TG

Sample	$T_{1\%}$ (°C)	$T_{3\%}$ (°C)	$T_{5\%}$ (°C)	$T_{10\%}$ (°C)	$T_{20\%}$ (°C)
1	112	175	195	233	267
2	136	197	226	255	282
3	145	199	227	256	285
4	120	178	198	230	258

version and the reason is probably due to the presence of the P—O—C structure in the main chain, which is very susceptible to chain scission during thermal degradation and acts as a weak link.[9] In an another study, Javni et al. determined the value of the average activation energy for the decomposition of vegetable oil-based PURs on the basis of isothermal and dynamic measurement.[10] The variation of activation energy demonstrated the complexity of the process—at the early stage urethane bond dissociation dominates, then the polyol component may contribute to a weight loss at higher conversions, causing an increase of E_a by 15 kJ/mol. The effects of different phosphonates and phosphates on the mechanism and kinetics of the decomposition reactions of rigid PUR foams, based on a polyol component obtained from by-products of the synthesis of dimethyl terephthalate and polymeric MDI, have been studied by Gjurova et al.[11] It was found that at the initial stage of decomposition the presence of additive in low concentrations does not affect E_a substantially, while for the second stage it increases by ca. 30 kJ/mol. It is noteworthy that all the described works do not yield information about the value of the preexponential factor and reaction model, which are crucial for an overall kinetic description. Hence, our approach is based on the reaction expressed by the stoichiometric equation:

$$A_{solid} \rightarrow B_{solid} + C_{gas}$$

The rate of reaction can be described in terms of two functions: $k(T)$ and $f(\alpha)$. Thus

$$\frac{d\alpha}{dt} = k(T)f(\alpha) \tag{1}$$

where α is the degree of conversion, $f(\alpha)$ is the type of reaction, and $k(T)$ is the rate constant.

By substitution of the Arrhenius equation [$k(T) = A \exp(-E_a/RT)$] the following equation results:

$$d\alpha/dt = A\exp(-E_a/RT)f(\alpha) \tag{2}$$

After introduction of the constant heating rate $\beta = dT/dt$ and rearrangement, we obtain

$$\frac{d\alpha}{f(\alpha)} = \left(\frac{A}{\beta}\right)\exp\left(-\frac{E_a}{RT}\right)dT \tag{3}$$

where T is the temperature in Kelvin, E_a the activation energy, A the preexponential factor, and R - the gas constant.

A subsequent integration of eq. (3) leads to the equation

$$G(\alpha) = \int_0^{\alpha} \frac{d\alpha}{f(\alpha)} = \frac{A}{\beta}\int_{T_0}^{T} \exp\left(\frac{-E_a}{RT}\right)dT \tag{4}$$

which cannot be expressed by a simple analytical form since its right-hand side corresponds to a series of infinite γ functions. In mathematical practice, logarithms are taken:

$$\ln G(\alpha) = \ln\left(\frac{A\,E_a}{R}\right) - \ln\beta + \ln p(x) \tag{5}$$

and exponential integral $p(x)$ is introduced:

$$p(x) = \frac{e^{-x}}{x} - \int_{\infty}^{x} \frac{e^{-x}}{x}\,dx \tag{6}$$

where $x = E_a/RT$.

Using an approximation of the exponential integral in a form proposed by Doyle,[12]

$$\ln p(x) = -5.3305 + 1.052x \tag{7}$$

it is possible to determine the activation energy of the thermal process by following the specific heat flow of a process at several different heating rates:

$$\ln\beta = \ln\left(\frac{AE_a}{R}\right) - \ln G(\alpha) - 5.3305 + 1.052x \tag{8}$$

Equation (8) generates a straight line when $\ln(\beta)$ is plotted against $1/T$ for isoconversional fractions, the slope of the line being equal to $-1.052E_a/R$ during a series of measurements with a heating rate of $\beta_1 \ldots \beta_j$ at a fixed degree of conversion of $\alpha = \alpha_k$. The temperatures T_{jk} are those at which the conversion α_k is reached at a heating rate of β_j. This method was developed independently by Ozawa[13] and Flynn and Wall.[14]

Another isoconversional procedure, introduced by Friedman,[15] use as its basis the following relationship:

$$\ln\left(\frac{d\alpha}{dt}\right) = \ln f(\alpha) + \ln A - \frac{E_a}{RT} \tag{9}$$

TABLE IV
Kinetic Model Functions[17]

Model	Symbol	$f(\alpha)$
Phase boundary-controlled reaction (contracting area)	R2	$(1-\alpha)^{1/2}$
Phase boundary-controlled reaction (contracting volume)	R3	$(1-\alpha)^{2/3}$
Random nucleation, unimolecular decay law	F1	$(1-\alpha)$
Reaction nth order	Fn	$(1-\alpha)^n$
Johnson–Mehl–Avrami	JMA	$n(1-\alpha)[-\ln(1-\alpha)]^{1-1/n}$
Two-dimensional growth of nuclei (Avrami equation)	A2	$2[-\ln(1-\alpha)^{1/2}](1-\alpha)$
Three-dimensional growth of nuclei (Avrami equation)	A3	$3[-\ln(1-\alpha)^{2/3}](1-\alpha)$
One-dimensional diffusion	D1	$1/(2\alpha)$
Two-dimensional diffusion	D2	$1/[-\ln(1-\alpha)]$
Three-dimensional diffusion (Jander equation)	D3	$3(1-\alpha)^{2/3}/2[1-(1-\alpha)^{1/3}]$
Three-dimensional diffusion (Ginstling–Brounshtein)	D4	$3/2[(1-\alpha)^{-1/3}-1]$
n-Dimensional nucleation (Avrami–Erofeev equation)	An	$n[-\ln(1-\alpha)^n](1-\alpha)$
Reaction of first order with autocatalysis	C1	$(1-\alpha)(1+K_{kat}\alpha)$
Reaction of nth order with autocatalysis	Cn	$(1-\alpha)^n(1+K_{kat}\alpha)$
Prout–Tompkins equation	Bna	$(1-\alpha)^n\alpha^a$

which makes it possible to find the activation energy value from the slope of the line ($m = -E_a/R$) when $\ln(d\alpha/dt)$ is plotted against $1/T$ for isoconversional fractions.

In eq. (1) term $f(\alpha)$ represents the mathematical expression of the kinetic model. The most frequently cited basic kinetic models are summarized in Table IV.

Nonisothermal curves of a thermal reaction can satisfy the kinetic equations developed for the kinetic analysis of "nth order reactions," even if they follow a quite different mechanism. Results of the comparative studies lead to the conclusion that the actual mechanism of a thermal process cannot be discriminated from the kinetic analysis of a single TG trace.[16] Besides, both the activation energy and preexponential factor, given in eq. (2), may be mutually correlated. As a consequence of this correlation, any TG curve can be described by an apparent kinetic model instead of the appropriate one for a certain value of apparent activation energy. Therefore, the kinetic analysis of TG data cannot be successful unless the true value of the activation energy is known.[17–19]

Activation energy and preexponential factor were determined by the Ozawa–Flynn–Wall method for sample 1 (Figs. 3 and 4).

We can observe that for $0.1 < \alpha < 0.4$ both the activation energy and preexponential factor remain stable at the level of app. 155 kJ/mol and 13 (log A), respectively. It may indicate that the mechanism of decomposition does not change at this conversion range and further kinetic modeling may be applied.

Activation energy and frequency factor values vs degree of conversion for samples 2– 4 are displayed in Figures 5–7, respectively.

In a subsequent calculation procedure, the corresponding kinetic parameters are computed by nonlinear regression, which is the iterative calculation of the minimum sum of least squares (LSQ). According to the maximum likelihood theorem, the method is op-

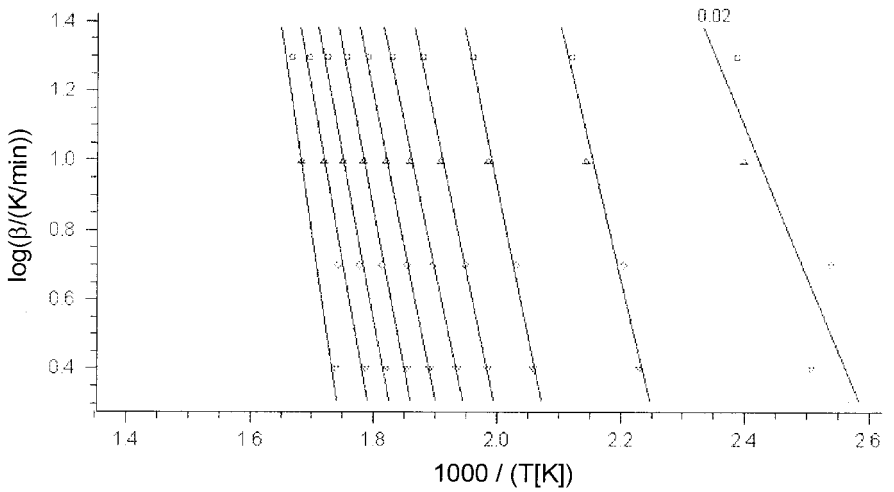

Figure 3 Ozawa–Flynn–Wall analysis of the decomposition process of sample 1.

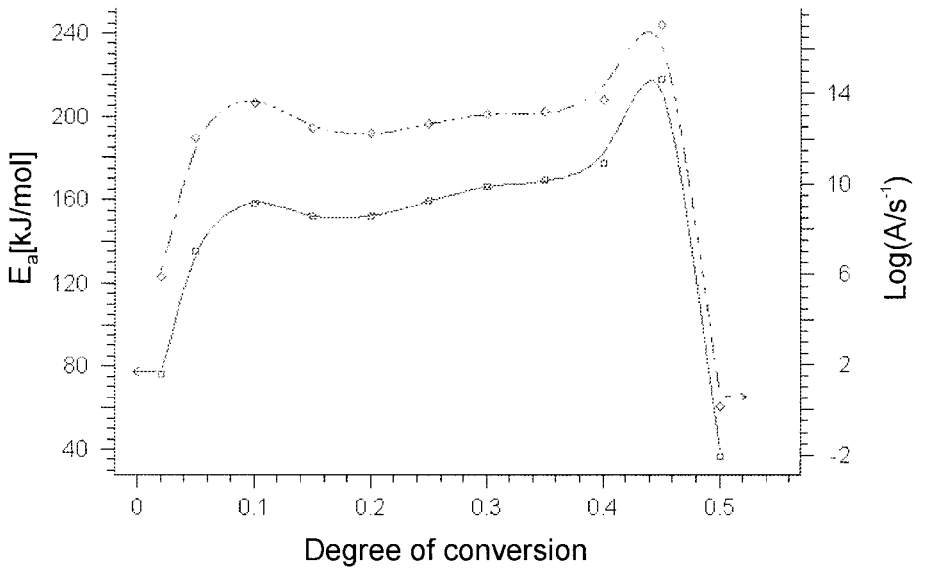

Figure 4 Activation energy (E_a) and preexponential factor (A) as a function of degree of conversion for the decomposition process of sample 1 calculated by the Ozawa–Flynn–Wall method.

timal when the weighting is carried out at the same time. Then, LSQ yields χ^2.[20]

$$LSQ = \sum_{j=1}^{S} \sum_{k=\text{Start}}^{\text{Fubak}_j} w_{j,k} \cdot (Y\exp_{j,k} - Y\text{cal}_{j,k})^2 \qquad (10)$$

where

$$w_{j,k} = \frac{\sum_{j=1}^{S} (\text{Final}_i - \text{Start}_i)}{S \cdot (\text{Final}_j - \text{Start}_j)} \cdot \frac{1}{S^2(Y\exp_{j,k}) + S^2(Y\text{cal}_{j,k})} \qquad (11)$$

and S is the number of measurements, j the curve index, Start_j the index of the point for which $x \geq x_{\text{Start}}$ is valid, Final_j the index of the point for which $x \leq x_{\text{Final}}$ is valid, $Y\exp_{j,k}$ the experimental value of curve j in points k, $Y\text{cal}_{j,k}$ calculated value for point j,k, $S^2(Y\exp_{j,k})$ the variance of the measured point j,k, and $S^2(Y\text{cal}_{j,k})$ the variance of the calculated point j,k.

Through the first term in eq. (11), each measurement enters LSQ with the same weight, independent from its number of points, N_j. Then, for the solution of the system of differential equations, a 5th-degree Runge–Kutta method (Prince–Dormand algorithm[21]) is employed as a subprogram. This subprogram is, for its

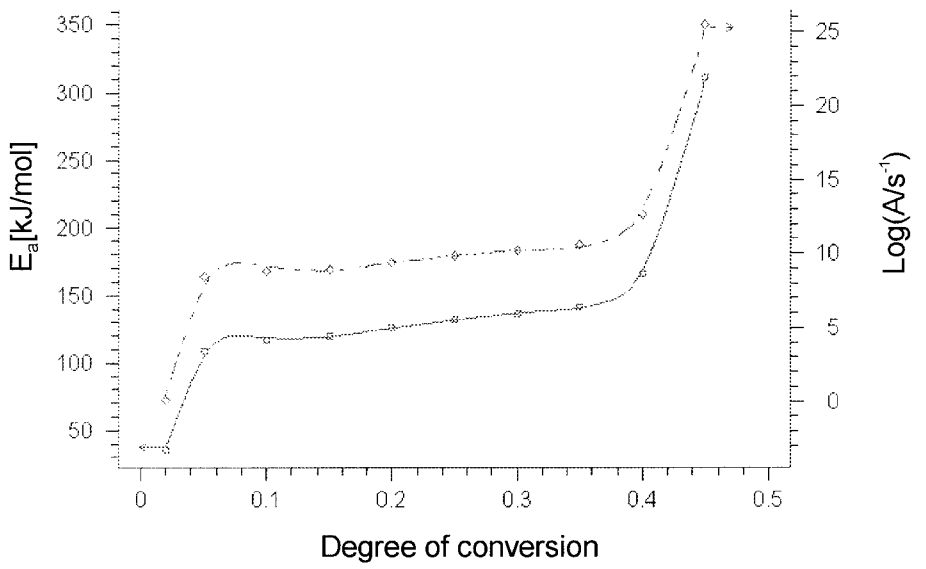

Figure 5 Activation energy (E_a) and preexponential factor (A) as a function of degree of conversion for the decomposition process of sample 2 calculated by the Ozawa–Flynn–Wall method.

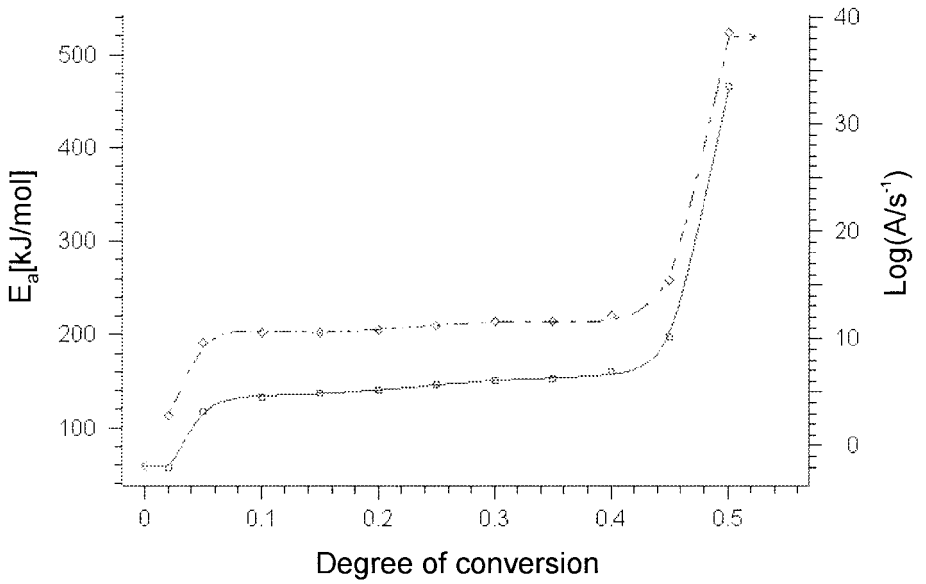

Figure 6 Activation energy (E_a) and preexponential factor (A) as a function of degree of conversion for the decomposition process of sample 3 calculated by the Ozawa–Flynn–Wall method.

part, tied into a hybrid regularized Gauss–Newton method.[22]

At the next stage F test,

$$F_{\exp}(f_1,f_2) = \frac{\sum_{j=1}^{S}\sum_{k=1}^{N_s}(Y_{jk} - \hat{Y}_{jk}(\text{model}_1))^2/f_1}{\sum_{j=1}^{S}\sum_{k=1}^{N_s}(Y_{jk} - \hat{Y}_{jk}(\text{model}_2))^2/f_2} \quad (12)$$

where $Y_{j,k}$, the measured value; $\hat{Y}_{j,k}$, the regress value; S, the number of scan; N_S, the number of measured values in the scan S; f_1, the degree of freedom of model 1; and f_2, the degree of freedom of model 2 (reference model) was applied to find best fit of $f(\alpha)$ functions. The esults of kinetic analysis are collected in Table V.

Comparison of the experimental data with theoretical (for models described by F test = 1.000) for samples 1–4 is shown in Figure 8.

As can be seen, the best approximation was found for a two-stage consecutive reaction, where the first step was the Avrami–Erofeev nucleation-dependent model and the second step was the chemical reaction (1st or nth order) model. Analyzing the origin of the first step, one should bear in mind that in deriving nucleation-dependent kinetic models, e.g., the Avrami–Erofeev model, it was assumed that the rate of nucleus formation depends on the number of energetically favorable sites (mostly depending on defects that are introduced during a thermal event). Nucleation of product N is followed by its growth G, which can have the character either of a surface chemical reaction or of diffusion. To calculate the volume of nuclei capable of further growth, usually a three-dimensional isotropic growth controlled by surface reaction is considered. An additional feature of an Avrami–Erofeev model is that it involves description of possible intergrowth of nuclei, i.e., a process in which the number of nuclei cannot increase unrestrictedly as the nuclei necessarily meet during their spatial growth and their growth is thus stopped. The overall activation energy of a nucleation-growth process is the sum of the partial energies of nucleation, growth, and diffusion, and that the exponent depends on the shape of the nuclei and the dimensionality of their growth, as well as on the rate of their formation. On the other hand, the preexponential factor depends on the geometry and number of sites capable of nucleation.[23] We should, however, bear in mind that kinetic model functions are based on physical-geometrical assumptions of regularly shaped bodies that are required to account for polydispersity, shielding and overlapping, unequal mixing and/or nonregular shapes, and anisotropy. The prolonged reaction tails due to the actual behavior of real particles and the particle nonsphericity in view of morphology description in terms of characteristic dimensions (usually the longest particle length), interface (average boundary line), and volume (mean section area) contribute to the complex behavior of a macromolecular system.

The fits of experimental data are quite good when two consecutive reactions are considered. With regard to $f(\alpha)$, it is possible to distinguish between the results obtained with the An function $[f(\alpha) = n[-\ln(1-\alpha)^n](1-\alpha)]$ and F_1/F_n function $[f(\alpha) = (1-\alpha)$ or $(1-\alpha)^n]$. The granular structure of additives facilitates nucleation growth of a polymer–additive system; then, at tem-

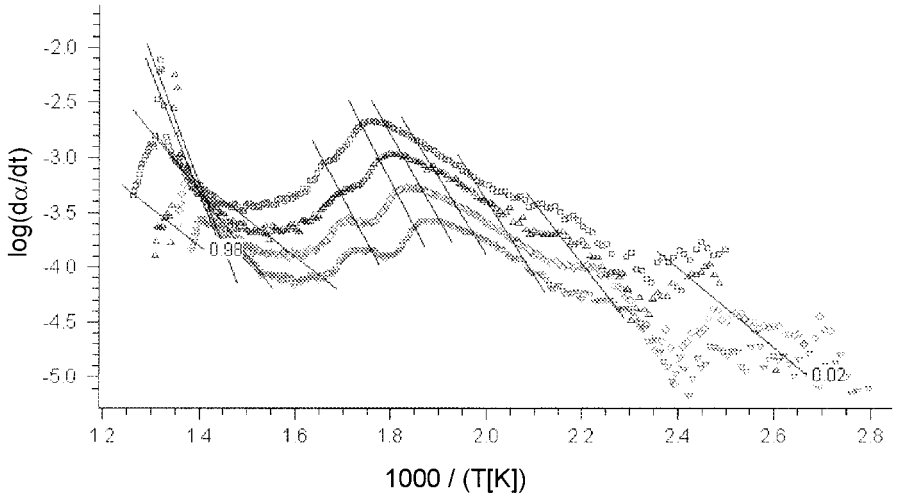

(a)

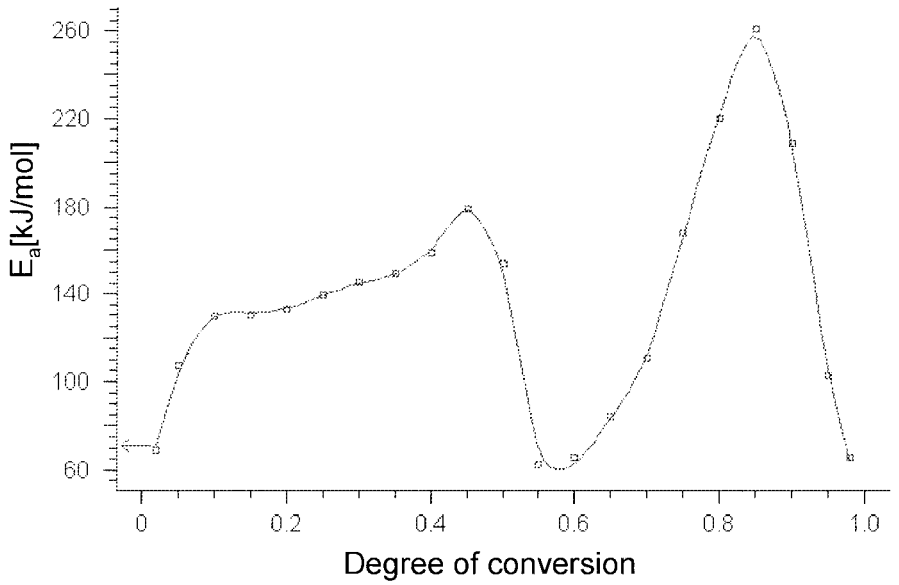

(b)

Figure 7 (a) Friedman analysis of the decomposition process of sample 4. (b) Activation energy (E_a) as a function of degree of conversion for the decomposition process of sample 4 calculated by the Friedman method.

peratures higher than 400°C chemical decomposition reaction becomes a kinetically dominating process. The stabilizing action of phosphate-based additives may be explained by the formation of surface-localized spherical barriers that are growing according to the nucleation growth mechanism and that attenuate the transfer of heat from the decomposition zone to the substrate. For the carbonate action, we can consider a twofold effect: influence of loosely bounded crystallized water and evolution of carbon dioxide that forms a air barrier at the polymer surface; the latter effect was found as dominating in the flame-retardancy mode of action. An additional role may be ascertained to the metal ion–polymer functional groups interaction that should lead to the formation of the long-range structural regularities that, in turn, thermally stabilize the whole system ("strong interactions model").

Proper kinetic parameters enabled us to show the behavior of the stabilized PUR systems under isothermal conditions (Figs. 9 and 10).

It can be seen from the kinetic simulation that addition of sodium dihydrogenphosphate increases the thermal stability of PUR foam at initial temperatures of decomposition.

Such a display of the process' parameters in the extrapolated range on the basis of calculated kinetic data may serve as a valuable tool for modeling, thus completing time- and energy-consuming experiments.

TABLE V
Results of the Kinetic Analysis

Sample	Model	log A_1	E_{a1} (kJ/mol)	Order	log A_2	E_{a2} (kJ/mol)	Order	F test
1	An An	17.20	210.1	0.23	8.32	164.0	0.89	1.584
1	An F1	12.41	158.6	0.31	5.99	127.0	—	1.000
1	An F1	8.98	121.4	0.45	5.05	116.4	—	1.297
2	An Fn	8.53	116.5	0.53	3.72	98.0	0.44	1.000
2	An F1	10.15	133.5	0.46	5.38	120.0	—	1.360
3	An D1	13.75	171.4	0.37	7.81	159.5	—	1.513
3	An An	13.85	173.8	0.34	7.92	155.1	0.93	1.774
3	An F1	9.97	132.1	0.46	5.02	114.4	—	1.000
4	An Fn	11.16	142.1	0.38	6.55	127.1	0.28	1.000
4	An F1	10.11	130.4	0.45	6.53	124.9	—	1.339
4	An F1	10.26	131.4	0.45	5.34	108.7	—	2.447

Examination of the volatile products

Considerably more information can be obtained if the coupling of TGA with evolved product analysis performed with FTIR is used. A unique feature of this system is its ability to provide continuous monitoring of the IR spectra of evolving product as well as quantitative analysis of gases. In contrast to pyrolysis GC, in which all the gases produced by heating to a given temperature are separated and analysed as a batch; TG/FTIR offers the great advantage of sequentially identifying the gases for a comprehensive vapor-phase analysis.

Analysis of the FTIR spectra reveals that there are several characteristic absorption bands in all systems under investigation—namely around 3600 cm^{-1} (—OH stretching), 2364 cm^{-1} (CO_2 stretching), 1760 cm^{-1} (C═O stretching), 1650–1550 cm^{-1} (NH bending and double bond sequences) (Fig. 11).

Evolution of CO_2, with a strong absorption band at 2364 cm^{-1}, can be followed over the whole process by analysis of a Gram–Schmidt chromatogram (Fig. 12).

On the basis of TG/FIR measurements, we can assume that the degradation reaction proceeds mainly via formation of carbon dioxide (route II in Scheme 1).

There have been evidence found for each of the mechanisms outlined in Scheme 1.[24] It may be also postulated that at a certain stage of thermal dissociation not only one degradation process occurs—such "mixed" mechanisms are often the rate-determining factors in case of many solid state reactions.

Diffuse reflectance infrared fourier spectroscopy

Diffuse reflectance infrared Fourier spectroscopy (DRIFTS) is a versatile technique that offers several significant advantages over conventional methods of

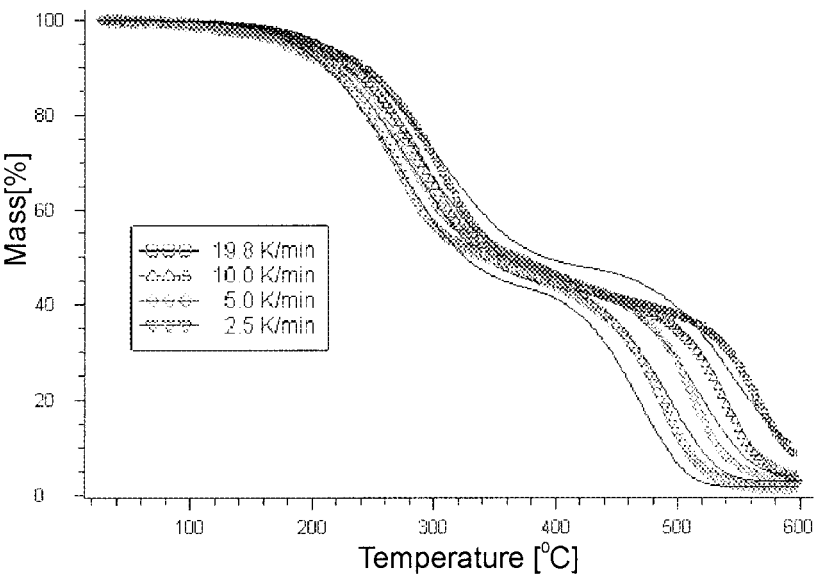

Figure 8 Comparison of the theoretical fits and experimental data for the decomposition of sample 1.

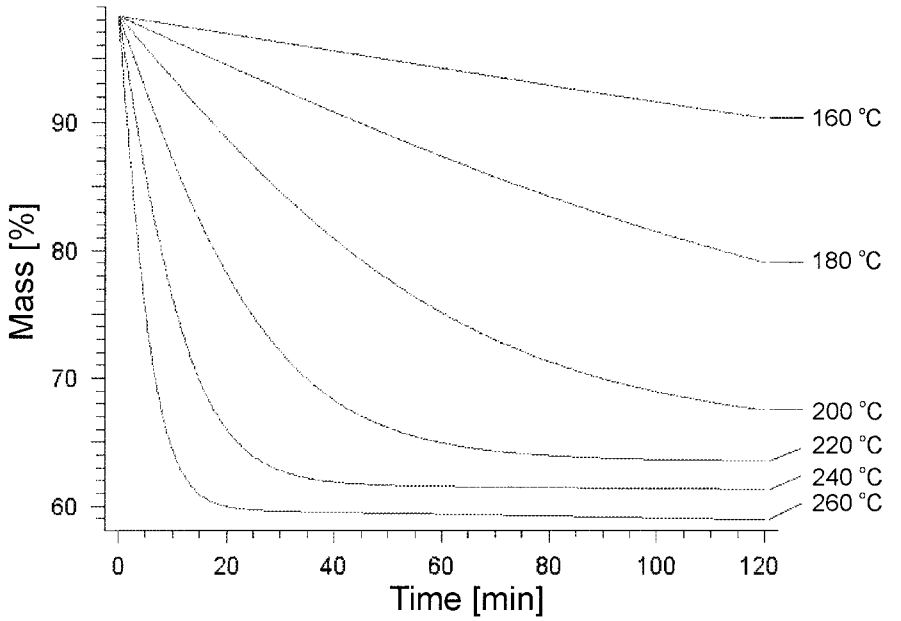

Figure 9 Simulation of isothermal decomposition of sample 1 on the basis of kinetic parameters obtained.

sampling solids. Some of these include the following: (1) minimal sample preparation and resulting therefrom no introduction of structural changes, (2) a very high sensitivity, and (c) a possibility of taking spectra from foams, fibers, and coatings without prior special preparation of the sample.[25,26]

Spectra of sample 1, taken after heating up to temperatures from ambient to 290°C, are presented in Figure 13.

We can observe an increase in intensity of bands in the carbonyl region at 1730 cm^{-1} and a decrease of saturated CH_2 deformations at 1250–1320 and 770–830 cm^{-1} for thermally treated samples. Similar effects were also observed for modified PUR samples, e.g., sample 2 (Fig. 14).

An additional weak peak at 2350 cm^{-1} for samples thermally treated may be assigned to CO_2, which is adsorbed on the degraded polymer surface; besides, formation of double bond sequences can be evidenced by increase of absorption at 1650–1600 cm^{-1}. These observations would confirm mechanism II in Scheme 1.

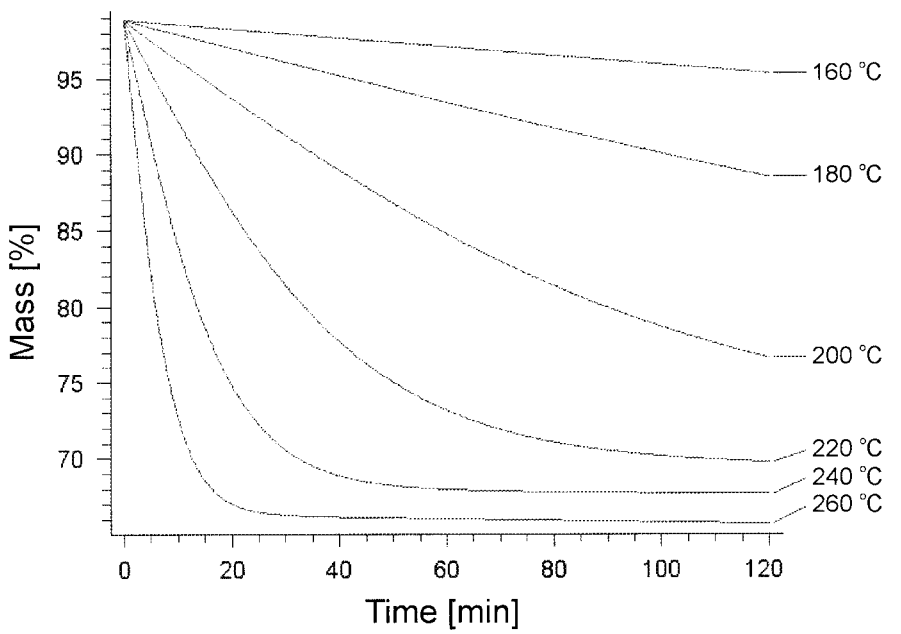

Figure 10 Simulation of isothermal decomposition of sample 2 on the basis of kinetic parameters obtained.

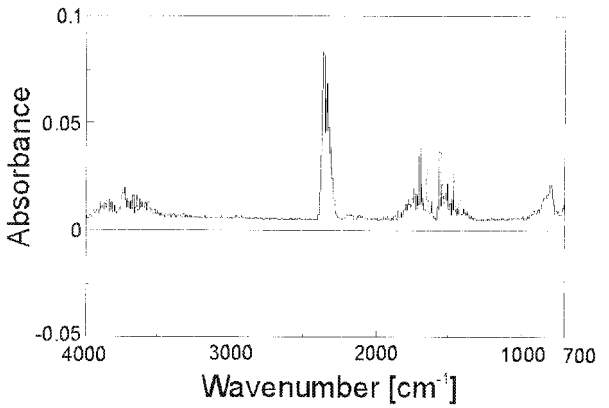

Figure 11 FTIR spectrum of the volatile products after 880 s of sample 4.

CONCLUSIONS

From the TG results it can be seen that both in air and nitrogen atmospheres there was an increase of the onset temperatures of decomposition; DTG maxima were also shifted toward higher temperatures as a result of stabilizing action of additives applied that facilitate formation of barriers that attenuate the transfer of heat from the decomposition zone to the substrate. Advanced kinetic analysis makes it possible to determine kinetic parameters and model functions over the whole range of conversion. For phosphate-stabilized PUR samples, E_a remains stable over a broad area of the degree of conversion, while for carbonate-containing sample two regions of E_a were observed. Further kinetic analysis by nonlinear regression revealed the form of kinetic function that was the best approximation for experimental data—for a two-stage consecutive reaction the first step was an Avrami–Erofeev nucleation-dependent model and the

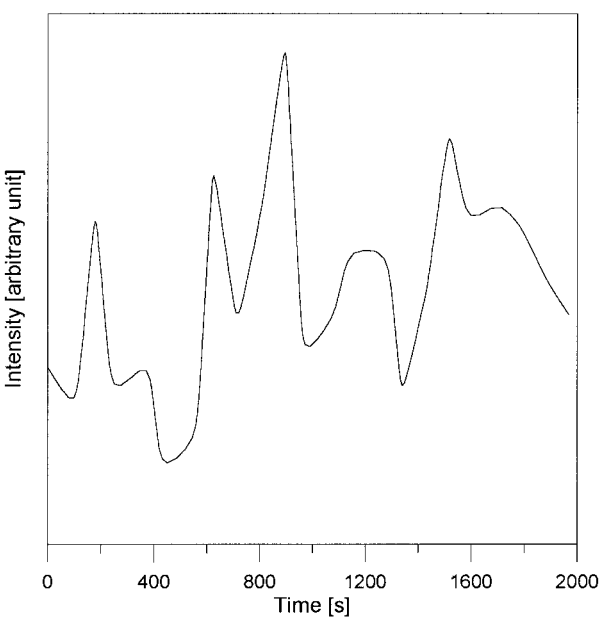

Figure 12 Intensity of CO_2 emission during the decomposition process of sample 4.

I. Dissociation to isocyanate and alcohol

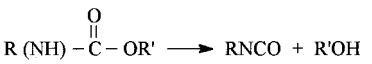

II. Formation of primary amine and olefin

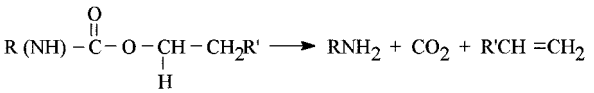

III. Formation of secondary amine

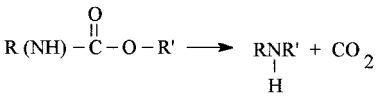

IV. Transesterification type bimolecular displacement

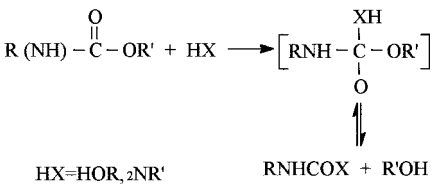

Scheme 1

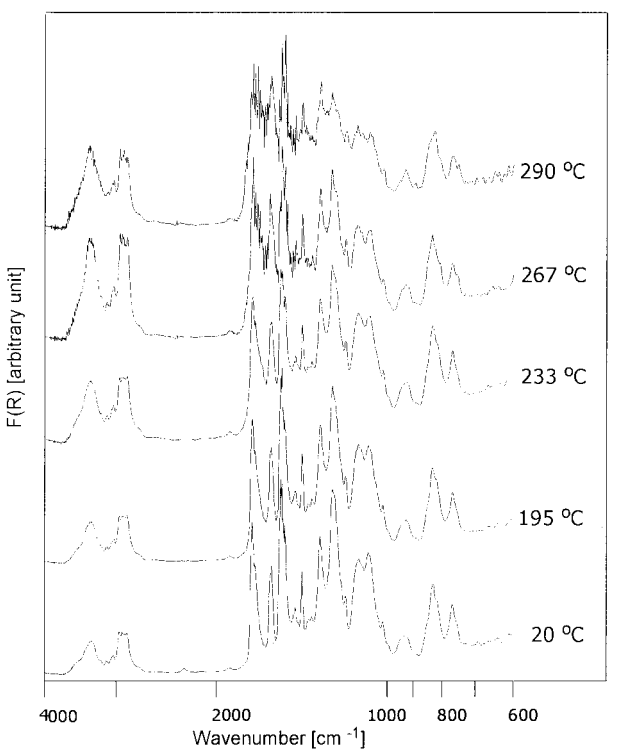

Figure 13 DRIFT spectrum of sample 1 thermally treated at temperatures indicated.

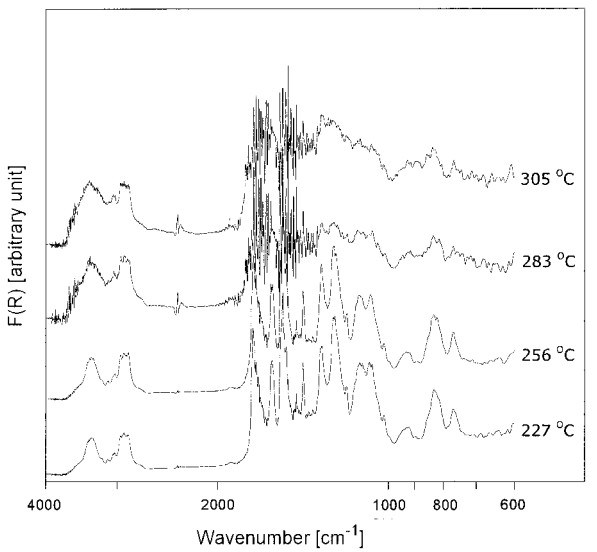

Figure 14 DRIFT spectrum of sample 2 thermally treated at temperatures indicated.

second step was a chemical reaction (1st or *n*th order) model.

The granular structure of these additives facilitates nucleation growth of a polymer–additive system, then, at temperatures higher than 400°C chemical decomposition reaction becomes a kinetically dominating process. In order to gain an additional look into the mechanism of decomposition, hyphenated TG/FTIR analysis was performed; results indicate that the prevailing mechanism of decomposition includes formation of carbon dioxide; from DRIFTS measurements of the solid residue one can observe decomposition of the urethane groups (in the carbonyl region) and formation of amine-containing species.

Samples of phosphates were kindly donated by Chemical Works ALWERNIA, Poland. We thank Prof. Edward D. Weil for useful discussions and help with DRIFTS measurements, and Prof. Edith A. Turi of the Polytechnic University for the kind use of thermal analysis equipment.

References

1. Gunter, O. Polyurethane Handbook; Carl Hanser Verlag: Muenchen, 1994.
2. Wirpsza, Z. Poliuretany. Chemia, technologia i zastosowanie; WNT: Warszawa, 1991.
3. Bayer, O. Das Diisocyanate-Polyadditions Verfahren; Carl Hanser Verlag: Munich, 1963.
4. Ravey, M.; Keidar, I.; Weil, E. D.; Pearce, E. M. J Appl Polym Sci 1998, 68, 217.
5. Camino, G.; Costa, L.; Luda di Cortemiglia, M. P. Polym Deg Stab 1991, 33, 131.
6. Grassie, N.; Zulfiqar, M. In Developments in Polymer Stabilization; Scott, G., Ed.; Kluwer Academic Publishers: Dordrecht, 1979.
7. Benbow, A. W.; Cullis, C. F. Combust Flame 1975, 24, 217.
8. Chang, T. C.; Chiu, Y. S.; Chen, H. B.; Ho, S. Y. Polym Deg Stab 1995, 47, 375.
9. Shankwalkar, S. G.; Cruz, C. Ind Eng Chem Res 1994, 33, 740.
10. Javni, I.; Petrovic, Z. S.; Guo, A.; Fuller, R. J Appl Polym Sci 2000, 77 1723.
11. Gjurova, K.; Troev, K.; Bechev, C.; Borisov, G. J Therm Anal 1987, 32, 97.
12. Doyle, C. D. J Appl Polym Sci 1962, 6, 639.
13. Ozawa, T. Bull Chem Soc Jpn 1965, 38, 1881.
14. Flynn, J. H.; Wall, L. A. Polym Lett 1966, 4, 232.
15. Friedman, H. L. J Polym Sci 1965, C6, 175.
16. Opfermann, J.; Kaisersberger, E. Thermochim Acta 1992, 203, 167.
17. Sestak, J. Thermophysical Properties of Solids, Their Measurements and Theoretical Thermal Analysis; Elsevier: Amsterdam, 1984.
18. Sestak, J.; Malek, J. Solid State Ionics 1993, 63–65, 245.
19. Pielichowski, K. Solid State Ionics 1997, 104, 123.
20. Christian, S. D.; Tucker, E. R. Internat Laboratory 1984, March, 10.
21. Engeln-Müllges, G.; Reuter, F. Formelsammlung zur Numerischen Mathematik; Bibliographisches Institut & F. A. Brockhaus AG: Mannheim, 1991.
22. Opfermann, J. J Therm Anal, submitted.
23. Allnat, A.; Jacobs, P. W. M. Can J Chem, 1968, 46, 111.
24. Yang, W. P.; Macosko, C. W.; Wellinghof, S. T. Polymer 1986, 27, 1235.
25. Yang, C. Q. Appl Spectrosc 1991, 45, 102.
26. McKenzie, M. T.; Culler, S. R.; Koenig, J. L. Appl Spectrosc 1984, 38, 786.